ADVANCED MATERIALS
www.advmat.de

Eliminating the Adverse Impact of Composition Modulation in Perovskite Light-Emitting Diodes toward Ultra-High Brightness and Stability

Zhiqi Li, Zhiwei Ren, Qiong Liang, Patrick W. K. Fong, Jianjun Tian,* and Gang Li**

Excess ammonium halides as composition additives are widely employed in perovskite light-emitting diodes (PeLEDs), aiming to achieve high performance by controlling crystallinity and passivating defects. However, an in-depth understanding of whether excess organoammonium components affect the film physical/electrical properties and the resultant device instability is still lacking. Here, the trade-off between the performance and stability in high-efficiency formamidinium lead iodide ($FAPbI_3$)-based PeLEDs with excess ammonium halides is pointed, and the underlying mechanism is explored. Systematic experimental and theoretical studies reveal that excess halide salt-induced ion-doping largely alters the PeLEDs properties (e.g., carrier injection, field-dependent ion-drifting, defect physics, and phase stability). A surface clean assisted cross-linking strategy is demonstrated to eliminate the adverse impact of composition modulation and boost the operational stability without sacrificing the efficiency, achieving a high efficiency of 23.6%, a high radiance of 964 W sr^{-1} m^{-2} (The highest value for $FAPbI_3$ based PeLEDs), and a prolong lifetime of 106.1 h at large direct current density (100 mA cm^{-2}), concurrently. The findings uncovered an important link between excess halide salts and the device performance, providing a guideline for rational design of stable, bright, and high efficiency PeLEDs.

1. Introduction

Metal halide perovskites have emerged as one of the most promising light emitters due to their impressive properties, including low cost, easy fabrication, high color purity, and tunable spectra.[1–8] Thanks to the development of composition[9,10] and additive engineering strategies,[11,12] significant progress has been achieved in perovskite light-emitting diodes (PeLEDs) and yielded external-quantum efficiencies (EQE) over 28%.[13] Furthermore, benefiting from the ionic nature of perovskite, the facile low-temperature solution process is well compatible with large-scale industrial manufacturing. These excellent properties make PeLEDs a fierce competitor with existing LED materials (e.g., III–V semiconductors, organic molecules/polymer, and quantum dots) in lighting and displaying fields.[14,15] The nature of ions and polycrystallinity of the hybrid perovskite is highly dependent on the precursor components. Especially for the organic-inorganic hybrid halide species, the most significant distinction in film fabrication originates from the composition change of perovskite precursor, in which perovskite films of PeLEDs are commonly endowed with excess organic ammonium halide components to boost device performance.[16–18] Composition modulation of perovskite shows great potential in controlling crystallinity and passivating defects for both photovoltaic and PeLEDs applications due to its easy realization by changing fabrication methods (e.g., spin-coating, thermal evaporation, I_2 vapor exposure, etc.) or the precursor component ratio (e.g., lead halide or organic halides).[19–22] For PeLEDs, high EQE of three-dimensional (3D) green and blue PeLED have been reported by introducing extra organic halides to form quasi-core/shell passivated structures.[23–25] Likewise, excess formamidinium iodide (FAI) has been widely employed in the state-of-the-art near-infrared (NIR) formamidinium lead iodide ($FAPbI_3$) perovskite emitters to form large and well-passivated crystals.[16,26] Despite the reported high efficiency for these PeLEDs, the ion migration can be aggravated unintentionally due to excess incorporated mobile ions from composition modulation, which would accelerate device degradation and lower the operational

Z. Li, Z. Ren, Q. Liang, P. W. K. Fong, G. Li
Department of Electrical and Electronic Engineering
Photonic Research Institute (PRI)
Research Institute of Smart Energy (RISE)
The Hong Kong Polytechnic University
Hung Hom, Kowloon, Hong Kong 2766 5111, China
E-mail: zhiweipv.ren@polyu.edu.hk; gang.w.li@polyu.edu.hk
J. Tian
Institute for Advanced Materials and Technology
University of Science and Technology Beijing
Beijing 100083, China
E-mail: tianjianjun@mater.ustb.edu.cn

The ORCID identification number(s) for the author(s) of this article can be found under https://doi.org/10.1002/adma.202313981

DOI: 10.1002/adma.202313981

stability. To date, most research works about the role of extra organoammoniums are focused on their effect on the crystallization kinetics.[27–29] A deep understanding of excess organic component modulation-induced physical/electrical property changes and concomitant instability of PeLEDs is still lacking.

In this work, we demonstrated the composition modulation induced ion-doping in the state-of-the-art $FAPbI_3$ PeLEDs. Via experimental and computational studies, the impact of excess organic halides on the physical properties of perovskite films and the resultant instability of PeLEDs are revealed. It is found that the increased electron-richer state of moderately excess organic ammoniums effectively shifts the perovskite surface energetics and thus modulates the charge-carrier dynamics of PeLEDs. However, the generated shallow defects aggravate ion migration/accumulation and play an adverse role in the degradation of PeLEDs. Based on our findings, a surface clean assisted crosslinking post-treatment was designed and implemented, resulting in simultaneously achieving a high EQE of 23.6%, a high radiance of 964 W sr^{-1} m^{-2}, and a prolong half-lifetime of ≈106.1 h (under large direct-current current density of 100 mA cm^{-2}), representing the brightest value for stable-operational $FAPbI_3$ based PeLEDs.

2. Results and Discussion

For typical organic-inorganic hybrid PeLEDs, the fabrication of perovskite emitter usually involves the incorporation of excess organic halides. A number of studies on perovskite photovoltaics indicate that these excess ammonium halides would result in ion-doping of perovskite emitters and thus modulate the performance of PeLEDs.[30–33] To reveal this behavior in PeLEDs, we employed typical 3D $FAPbI_3$ as a model composition and fabricated PeLEDs with the structures of indium tin oxide (ITO)/ZnO/ethoxylated-polyethylenimine (PEIE)/ perovskite/ poly (9,9-dioctyl-fluorene -co-N-(4-butylphenyl) diphenyl-amine) (TFB)/MoO_3/Au. The perovskite emitters were prepared with the addition of different excess FAI amounts in the precursor mixture, and the detailed fabrication procedure is described in Experimental section. Meanwhile, a typical perovskite film used for perovskite solar cells (PSCs) was fabricated as a comparison based on our previous work.[34] For clarity, we name the as-prepared films as FAI-x in the following discussion, where x is the ratio of FAI/PbI_2 (x = 2, 2.2, 2.5, 3).

The genesis of this study began with the investigation on the energy levels of perovskite films through detecting the secondary electron cut-off region of ultraviolet photoelectron spectroscopy (UPS) spectrum. As shown in **Figure 1a**, the obvious left-shifted secondary electron cut-off edges were observed for FAI-2.0 films compared to the reference films (the stoichiometric $FAPbI_3$ films for PSCs, i.e., FAI-1.0). The edges further left-shifted with increasing excess FAI, suggesting that the excess ammonium halide components shifted the energy levels of the perovskite films. Figure 1b demonstrates the energy levels of perovskite films for PeLEDs from UPS and optical property measurements of perovskite films (Figure 1a; Figure S1, Supporting Information). The difference between the conduct band and Fermi level (E_C-E_F) in Figure 1c are 0.47, 0.39, 0.29, and −0.04 eV for FAI-2.0, 2.2, 2.5, 3.0 films, respectively. The E_F of the perovskite trends to up-shift toward E_C, suggesting a more negative work-function (W_F) shift of perovskite films.[35]

The change in surface potentials was further verified by Kelvin probe force microscopy (KPFM) measurements. Figure 1d and Figure S2 (Supporting Information) show the atomic force microscopy (AFM) topography and KPFM images. Morphology evolution of perovskite films is in good agreement with previous reports.[16] Notably, the electric potential tends to increase with the increased amount of excess FAI in the precursor. As a result, the calculated W_F also increases, which is well consistent with the UPS results. Given that electron-donating nitrogen of the ammonium groups makes FA^+ an overall electron-richer dopant, we speculated that the changed surface energetics of perovskite films results from the incorporated organic ammonium cation components.[36,37] To exclude the influence of iodine ions on the energy level shifting, we change the base $FAPbI_3$ composition with excess FABr instead of FAI. A similar trend was also observed from the UPS measurements (Figure S3, Supporting Information). The minor difference in the secondary electron cut-off edges can be linked to a relatively increased electron-withdrawing ability of the Br^- anion compared to that of I^- anion. Therefore, we attributed this shifted energy levels to the electron-richer role of extensively excess organic ammoniums.[38]

Figure 1e gives the distribution of EQE and radiance of PeLEDs with different excess FAI. Both EQE and radiance first increase and then decrease with the increasing excess FAI. To explore the reason of the performance variation, we first examined the morphology evolution and crystallinity of the perovskite films with different excess FAI. From AFM and scanning electron microscopy (SEM) images (Figure 1d; Figure S4, Supporting Information), the crystal sizes and surface coverage of the perovskite films with FAI from 2.0 to 2.5 negligibly changed. Further comparisons of the XRD spectra suggested that the crystallinity is similar for all the films (Figure S5, Supporting Information). Obviously, FAI-2.2 based PeLEDs exhibit an increase in device efficiency and radiance (Figure 1f; Figure S6, Supporting Information) compared to FAI-2.0. The enhanced EQE in a low current density range (Region I in Figure 1f) can be attributed to the better passivation of excess FAI. Meanwhile, the decreased efficiency roll-off can be connected with the optimized heterointerface charge transfer dynamics due to the different energy-level alignment. In fact, previous studies reported imbalanced charge injection inside of the state-of-the-art NIR PeLEDs, that is, hole injection ability is less efficient than electron injection ability. This unbalanced injection increases the carrier accumulation at the interfaces, thus causing an increased non-radiative recombination and degraded device performance.[39,40] Compared to FAI-2.0 films, a more negative W_F enhances hole injection (Figure S7, Supporting Information), which decreases the efficiency roll-off under large current density range (Region II) and achieves higher radiance. To verify the effect of energy level shifting on the carrier injection in PeLEDs, carrier-only devices were fabricated with the structure of ITO/ZnO/PEIE/Perovskite/LiF/Al and ITO/PEDOT:PSS/perovskite/TFB/MoO_3/ Al. As shown in Figure 1g, the hole current density of FAI-2.2 device shows an obvious enhancement compared with that of FAI-2.0, which balances the carrier injection on both sides and facilitates radiative recombination.[39] The decrease of carrier accumulation also

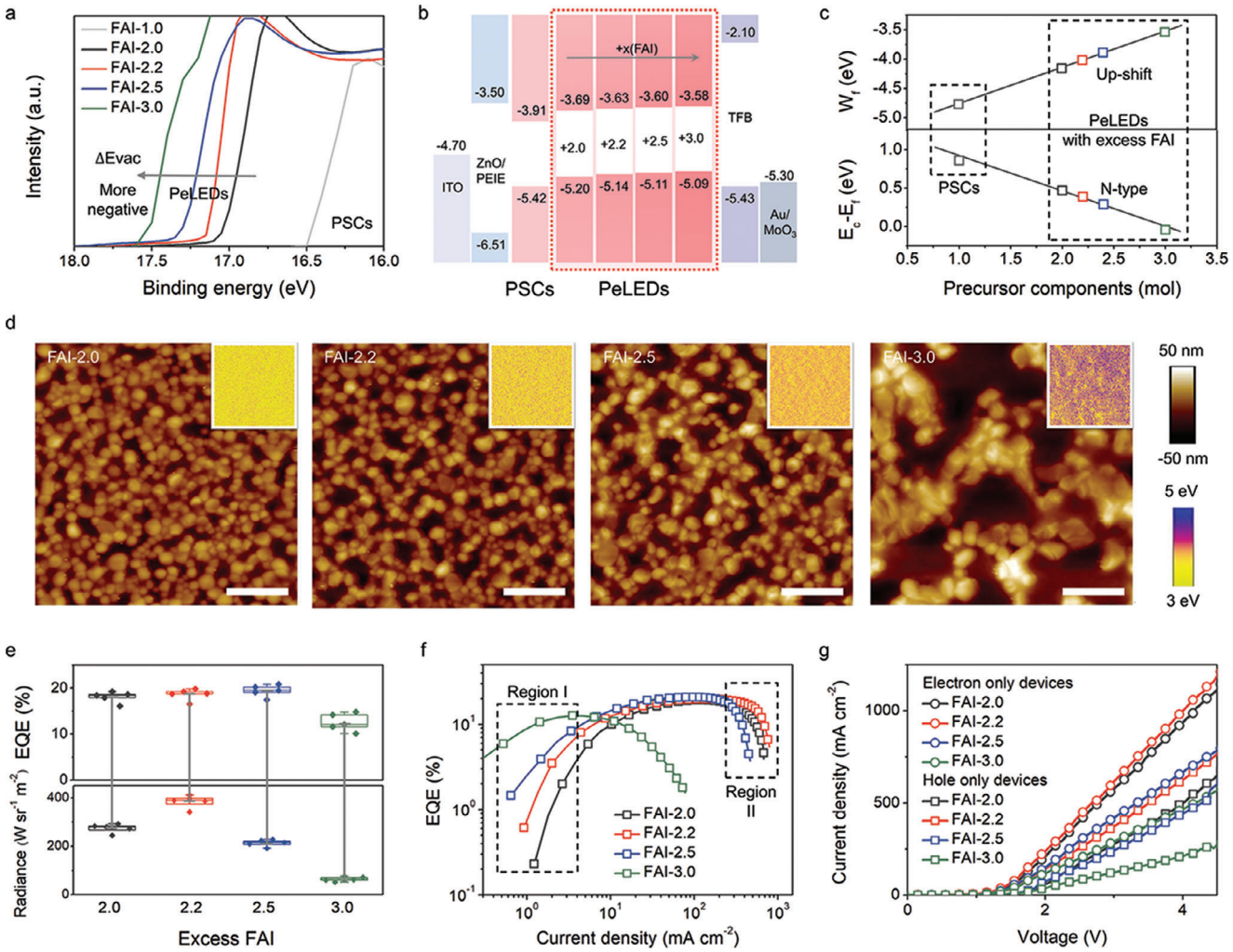

Figure 1. Perovskite film and device characteristics. a) UPS secondary electron cut-offs spectra of perovskite films with excess FAI. b) Schematic diagram of the energy levels for PeLEDs. c) W_F and E_C-E_F as a function of excess FAI. d) AFM topography images of the perovskite films. Insets, the corresponding KPFM surface potential maps. Scale bars: 1 μm. e) Distribution of EQE and radiance of PeLEDs. f) EQE-current density plots of PeLEDs. g) Current density-voltage plots of carrier-only devices.

reduces Auger recombination, thus suppressing the decrease of EQE at high current density that results in the low EQE roll-off.

It is observed that there is a significant fluctuation in the change of the device performance with further increasing excess FAI. As shown in Figure 1f and Figure S6 (Supporting Information), FAI-2.5 based device delivers the highest peak EQE operated at a lower current density, which can be attributed to the balanced injection (Figure 1g) and efficient defect passivation. As presented in Figure S8 (Supporting Information), the FAI-2.5 films show enhanced PL intensity compared with FAI-2.0 and FAI-2.2 films. High PL quantum yield (PLQY) of 69% is obtained for FAI-2.5 films compared to lower values of 42% for FAI-2.0 and 53% for FAI-2.2 films. Consistent with the PL and PLQY results, the time-resolved PL (TRPL) measurements show that the PL lifetime for FAI-2.5 films increases from 482 to 1881 ns, suggesting that excess organic halides passivate the defects in the resulting films.[11,12,16,22] We further compared the trap-filling limit voltage of devices and observed the variation of trap density (Figure S9, Supporting Information). The decreased trap-filling limit voltage for FAI-2.5 device indicated efficient defect passivation from excess FAI.[19,22] Compared to FAI-2.2 PeLEDs, both FAI-2.5 and 3.0 based devices exhibit lower radiance, which is caused by decreased injected current density and more severe efficiency roll-off. The former is related to the worse carrier injection due to decreased electric conductivity of excess organic residue. The significant decrease in current injection could increase interfacial nonradiative loss, thus reducing device radiance. The efficiency roll-off is attributed to the serious ion migration, which will be further explored in the following section.[40,41] Therefore, we ascribed this fluctuated performance of PeLEDs with excess FAI to the trade- off of carrier injection, defect passivation, and ion migration.

To demonstrate the influence of excess halides on ions migration and thus deteriorated roll-off, we performed the scan direction-dependent EQE and current density-voltage curves of the FAI-2.2 and FAI-2.5 devices (**Figure** 2a; Figure S10,

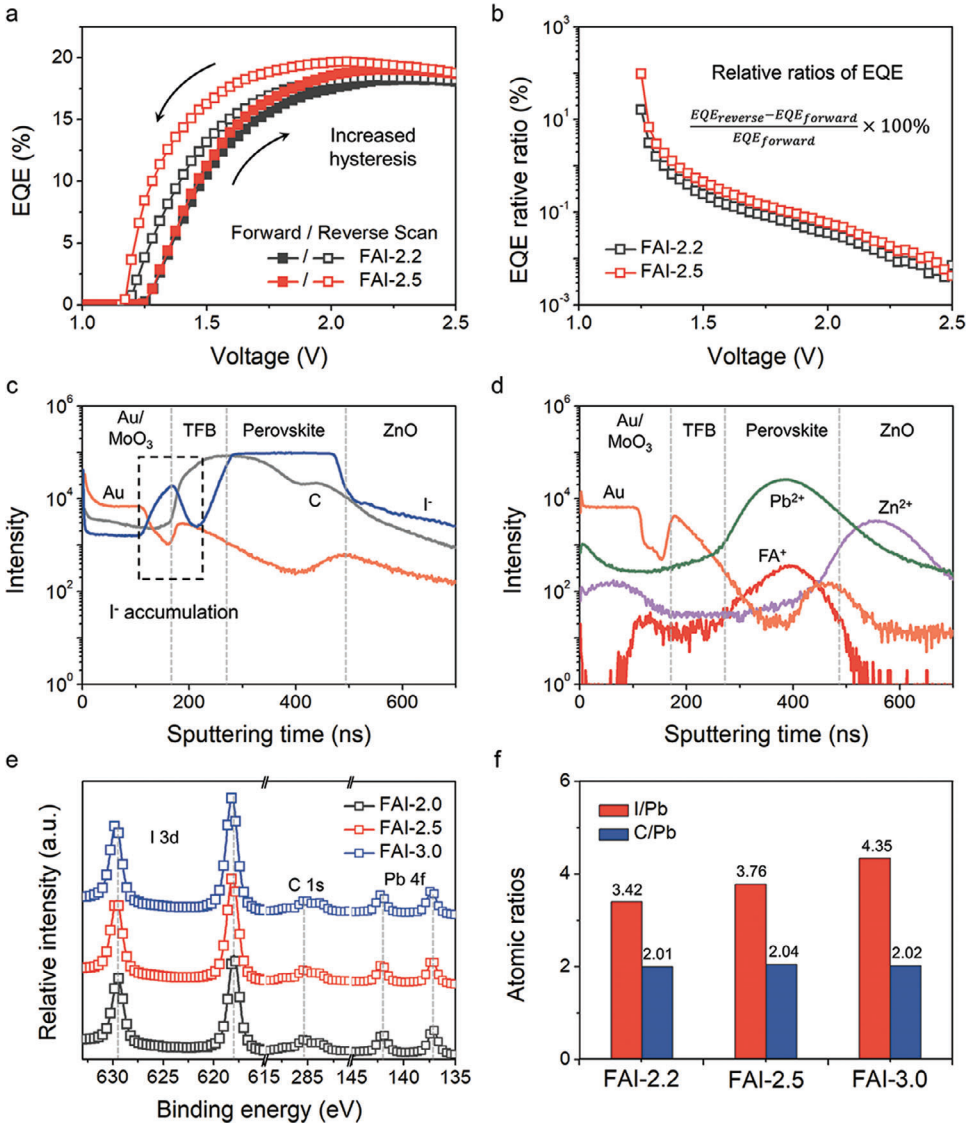

Figure 2. Effects of excess organic halides on ions migration. a) EQE-voltage curves of the FAI-2.2 and FAI-2.5 devices from forward and reverse scans. b) EQE relative ratios between reverse and forward scans. ToF-SIMS depth profiling of PeLEDs: c) Negative charge (I^-) detection. d) Positive charge (FA^+, Pb^{2+}, Zn^+) detection. e) XPS core-level spectra for I 3d and Pb 4f of FAI-2.2, FAI- 2.5, and FAI-3.0 films. f) The I/Pb and C/Pb ratios of FAI-2.2, FAI-2.5, and FAI-3.0 films.

Supporting Information).[40–42] It is found that FAI-2.5 based PeLEDs indeed show an increased EQE hysteresis between the forward and reverse scans compared to FAI-2.2 based PeLEDs (Figure 2b). Meanwhile, the scan direction-dependent current density-voltage hysteresis became more pronounced with the increased excess FAI. This aggravated hysteresis indicates that incorporated excess FAI could cause the trap states and increase ion migration owing to the fact that ion migration is a defect-dominated ionic behavior.

To identify whether both anions and cations play an identical role in ion migration, we performed time-of-flight secondary ion mass spectrometry (ToF-SIMS) depth profiling characterizations on the degraded 2.2-based PeLEDs. From ToF-SIMS results, we found that obvious I^- ions signals were collected in the interfacial region between Au/MoO_3 and TFB layer (Figure 2c), while no accumulation of FA^+ cations can be detected on the interface of perovskite and ZnO due to the large ionic radius of cations in PeLEDs (Figure 2d). The results imply that the negatively charged I^- ions play a dominant role in the field-dependent halide migration. X-ray photoelectron spectroscopy (XPS) measurements further revealed our conclusions. The core-level spectra of Pb element and I element for FAI-2.2, FAI- 2.5, and FAI-3.0 samples are shown in Figure 2e. A slight shift of Pb and I peak can be related to the passivation of organic halides. It is found that the intensity of I signal is much stronger than that of Pb signal and proportional to the increasement of the incorporated excess FAI. The elemental ratios of I/Pb were calculated by integrating peak area (Figure 2f). The calculated I/Pb ratios are 3.4, 3.8, and 4.3 for FAI-2.2, FAI-2.5, and FAI-3.0 samples, respectively. This enhancement in calculated I/Pb ratio indicates that the

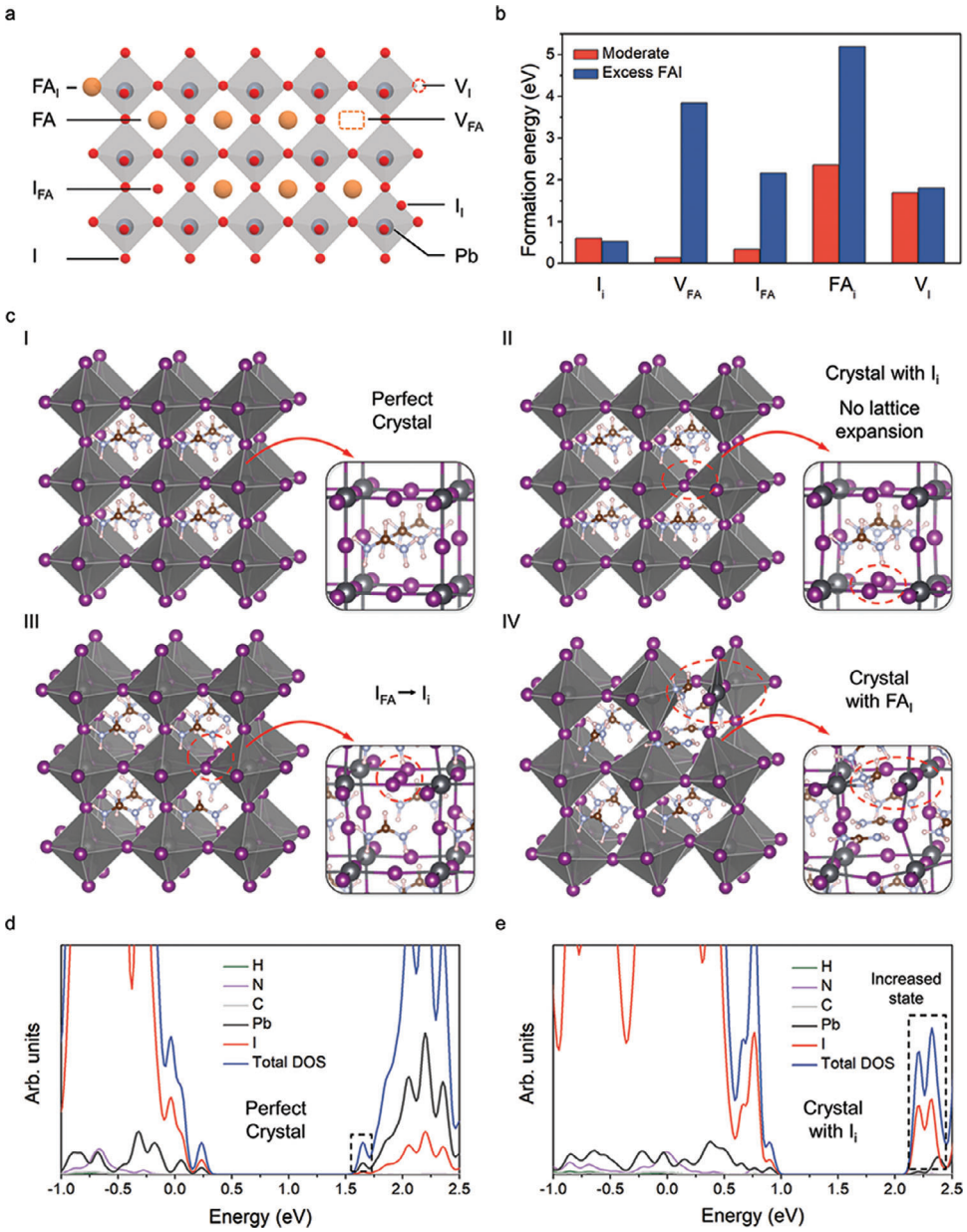

Figure 3. Theoretical calculations of the defects in PeLEDs. a) Schematic diagram of FAI-related point defects in $FAPbI_3$ perovskite. b) The calculated formation energies of point defects in $FAPbI_3$ under a stoichiometric and excess FAI condition. Bulk values of stoichiometric perovskite reproduced from Liu and Yam.[43] c) Geometric structure of perfect crystal and crystal with different defects. Calculated PDOS of perfect crystal (d) and crystal with iodine interstitial defects (e).

incorporated excess I^- anions offer a key source causing the severe ion migration.

Defects generation and reparation have been demonstrated to be the underlying mechanism of field-dependent ion drift and back-diffusion. Based on the knowledge of perovskite research, it is speculated that excess FAI inside of perovskite crystals possibly generates related defects (**Figure** 3a). Hence, first-principles density functional theory (DFT) calculations were performed to identify the potential defect species. The formation energies of FAI-related neutral point defects in $FAPbI_3$ under a stoichiometric and excess FAI condition were calculated. Figure 3b shows the bulk formation energies of the potential defects, including V_I, I_i, FA-I antisite defects (FA_I), and I-FA antisite defects (I_{FA}). By comparison, the calculated formation energies of defects in $FAPbI_3$ with excess FAI increased from 1.16 to 1.81 eV for V_I, 1.27 to 5.20 eV for FA_I, 0.54 to 3.85 eV for V_{FA} and 1.37 to 2.17 eV for I_{FA}, while it decreased from 1.13 to 0.53 eV for I_i.[43] Consequently, shallow iodine interstitial defects with relatively low formation energy are theoretically predicted to easily form inside the perovskite crystals with excess FAI.

The formation of shallow iodine interstitial defects was further rationalized by analyzing the geometric structure of crystals.

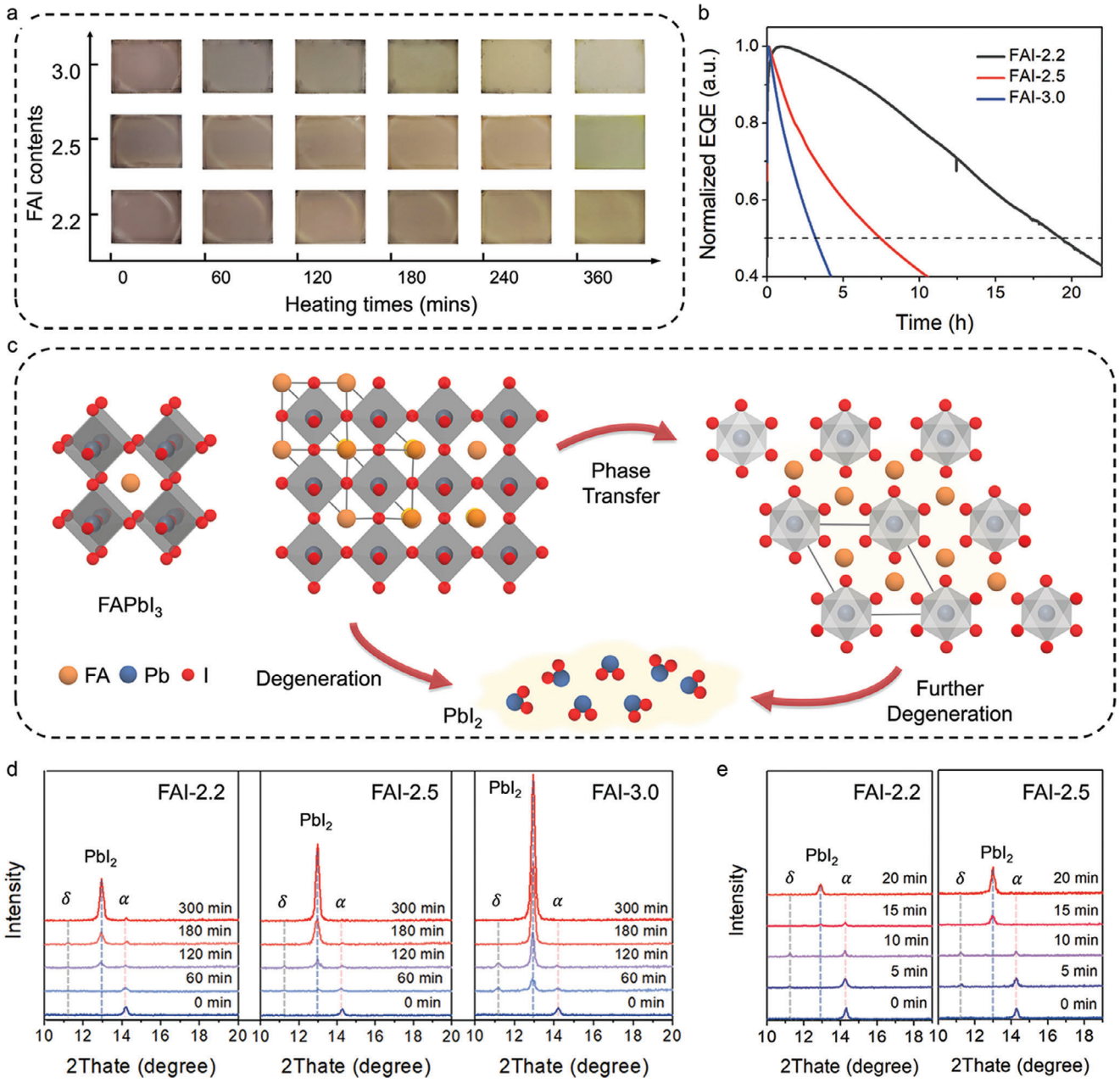

Figure 4. Stability of perovskite films and PeLEDs. a) Digital images of perovskite films with different excess FAI during thermal treatment for different time durations. b) T_{50} measurement under a constant current density of 100 mA cm^{-2}. c) Schematic diagram of perovskite phase transition. d) XRD patterns evolution of the corresponding perovskite films. α and δ denote the diffraction peaks of α-$FAPbI_3$ and δ-$FAPbI_3$, respectively. e) Evolution of XRD patterns of perovskite films after exposing the heat-treated films to I_2 vapor.

Compared with the perfect crystal structure (Figure 3c), the incorporation of I^- ions inside the crystal leads to negligible lattice distortion, which accounts for low formation energies of iodine interstitial defects. This negligible lattice shrinkage is consistent with the XRD experimental results, in which no peak shift can be seen, as in Figure S5 (Supporting Information). Notably, I^- in FA^+ site tends to enter the interstitial site, thus increasing iodine interstitial defects. Figure S11 (Supporting Information) compared the geometric structure of perovskite crystals with other defects, which further verified our conclusion. The partial density of states (PDOS) of pure and non-stoichiometric (with excess FAI) perovskite was calculated to gain a detailed understanding of the energy structure. As shown in Figure 3d,e, the energy levels shifted to higher binding energy due to the formed electronic states of iodine interstitial defects. Moreover, we find that the accumulated iodine states occur on the top of the valence band edge, which indicates that the negatively charged I_i^- state is a shallow trap state, which agrees with previous theoretical results from perovskite photovoltaics.[44] Despite the fact that the negatively charged I_i^- is identified as unintentionally impurity states,

the PL spectra (Figure S8, Supporting Information) exhibits an increasing intensity with the improving amount of excess FAI, suggesting that shallow iodine-related interstitial defects would not act as non-radiative trap states.

Although the unintentionally generated shallow defects do not act as non-radiative recombination centers, it has been shown that I_i defects diffuse to participate in the breakage and reformation of the lattice, which destroys the intrinsic stability of perovskite and accelerates self-degradation of perovskite photovoltaics. In fact, the situation would be more complicated due to the effect of illumination (self-absorption), oxygen, joule heating, and large operational bias.[45–47] Similar shallow defect-dominated degradation pathway might be observed for hybrid PeLEDs with excess organic halides due to the effect of ion migration and the joule thermal. Furthermore, recent reports have shown that PeLEDs are extremely sensitive to operational temperature. A slightly elevated temperature from self-heating could induce the degradation of light-emitting layers during operation, particularly for thermally unstable organic hybrid perovskites.[48,49]

To test whether shallow defects have a detrimental influence on $FAPbI_3$, we heat-treated perovskite films in a nitrogen glovebox and observed the change in the color of perovskite films. As shown in **Figure 4a**, the films exhibit obvious color fading during the thermal treatment, implying a phase transition in heat-treated perovskite films. Furthermore, the perovskite films demonstrate more obvious color fading with increasing excess FAI. We recorded the operational lifetime of FAI-2.2, FAI-2.5, and FAI-3.0 based PeLEDs in Figure 4b to study the device degradation trend. It is found that T_{50} of PeLEDs demonstrate a decreased trend with increased excess FAI, suggesting a negative effect of incorporated excess FAI on device stability. As shown in Figure 4c, I_i coordinates with Pb in a face-sharing configuration, which reduces the phase transition barrier and accelerates films degeneration.[44,45] To verify this degenerated process, we recorded the phase transfer of perovskite films during heat treatment. From Figure 4d, we find that all the films exhibit detectable and gradually increasing diffraction peaks of PbI_2., accompanied with the appearance of small δ peaks. PbI_2 -to-cubic α(100) XRD peak intensity ratio of perovskite films as a function of annealing time in Figure S12 (Supporting Information) indicates that the perovskite films demonstrate faster degeneration with increasing excess FAI.

Previous reports demonstrated that the excess iodine interstitial defects in the perovskite can undergo an autocatalytic chain reaction with self-generated I_2 vapor and cause an intrinsic degradation pathway. Therefore, the detrimental role of the generated iodine interstitial defects on film degradation would be able to be proved just by exposing the perovskite to excess I_2 vapor and observing accelerated degradation. By intentionally exposing the heat-treated perovskite films to additional I_2 vapor, we observed that the films degraded more rapidly with increased excess FAI (Figure 4e), which is attributed to an accelerated degeneration to PbI_2 due to the low phase transition energy barrier, consistent with previous reports.[45]

Our findings highlight the significant role of managing excess organic halide in improving device performance without scarifying device stability. We propose a surface clean assisted cross-linking strategy to simultaneously boost the PeLEDs electroluminescence performance and stability by removing excess mobile ions and passivating surficial defects (Figure S13, Supporting Information). The perovskite films were first treated with chloroform surface-washing to remove the excess FAI (Note S1, Supporting Information).[40] The decreased I^- signal intensity in the XPS spectra suggests that organic iodides are partially removed from perovskite emitter after chloroform post-treatment (Figure S14, Supporting Information). Next, a crosslinking-enabled interfacial molecular trimethylolpropane triacrylate (TMTA) was in situ cross-linked onto perovskite films as surface passivation agent (Note S2, Supporting Information).[50] Figure S15 (Supporting Information) presents PL spectra of perovskite with post-treatment, the surface clean-assisted cross-linking films show enhanced PL intensity compared with other films, suggesting efficient passivation in the resulting films.

Device performances of PeLEDs are exhibited in **Figures 5a–c** and S16 (Supporting Information). The optimized device shows a high peak EQE of 23.6%, which is substantially higher than that achieved for the control devices (peak EQE, 20.7%) and comparable with state-of-the-art near-infrared PeLEDs (Table S1, Supporting Information). The EQE distribution of PeLEDs is presented in Figure S17 (Supporting Information). Compared to the control one, the optimized devices are generally capable of achieving over 20% of EQE and up to more than 22%, which demonstrates better reproduction performance of PeLEDs. We note that the EQE values show a remarkable delay of roll-off at a large range of current density reaching 1500 mA cm^{-2}, thereby achieving an enhanced radiance of 964 W sr^{-1} m^{-2}, which is the highest value for FAPbI3 based PeLEDs with the EQE>20%.

To determine the operational lifetimes of optimized PeLEDs, accelerated aging tests were conducted at a high current density of 100 mA cm^{-2}. The maximum T_{50} lifetimes of the optimal device improve significantly (Figure 5d), showing a T_{50} of ≈106.1 h with initial radiance of ≈112 W sr^{-1} m^{-2}. In contrast, the control devices rapidly degraded with a T_{50} lifetime of ≈20.7 h under the same test conditions. Given that the surface clean assisted cross-linking post-treatment not only removes residual organic halide, but also blocks ions migration by passivating the surface defects,[51] we further solidify our results by performing ToF-SIMS depth profiling characterizations of the degenerated devices. We observe that an iodide accumulation signal at the interface between Au/MoO_3 and TFB layer (Figure 5e) is vanished for an optimized device, which agrees well with our expectation. Figure 5g compares the migration activation energy (E_a) of I^- from perovskite crystals. The E_a is ≈1.01 eV in the crystals with the existence of I_i defects, while it is 1.35 eV in perfect crystals. The small E_a accelerates ion migration and device degradation, damaging the device stability. We compared our device performance with the state-of-the-art $FAPbI_3$ based NIR PeLED, which is shown in Figure 5h and Table S1 (Supporting Information). Generally, the state-of-the-art $FAPbI_3$ PeLEDs with the peak EQE more than 20% reports low radiance (typically ≈300–500 W sr^{-1} m^{-2}) and a small operational lifetime (typically ≈1 – 30 h) operated at a high current density of 100 mA cm^{-2}.[8,11,12,18,19,39] Our surface clean assisted cross-linking post-treatment strategy provides an opportunity for these devices to simultaneously achieve high EQE, radiance, and stability.

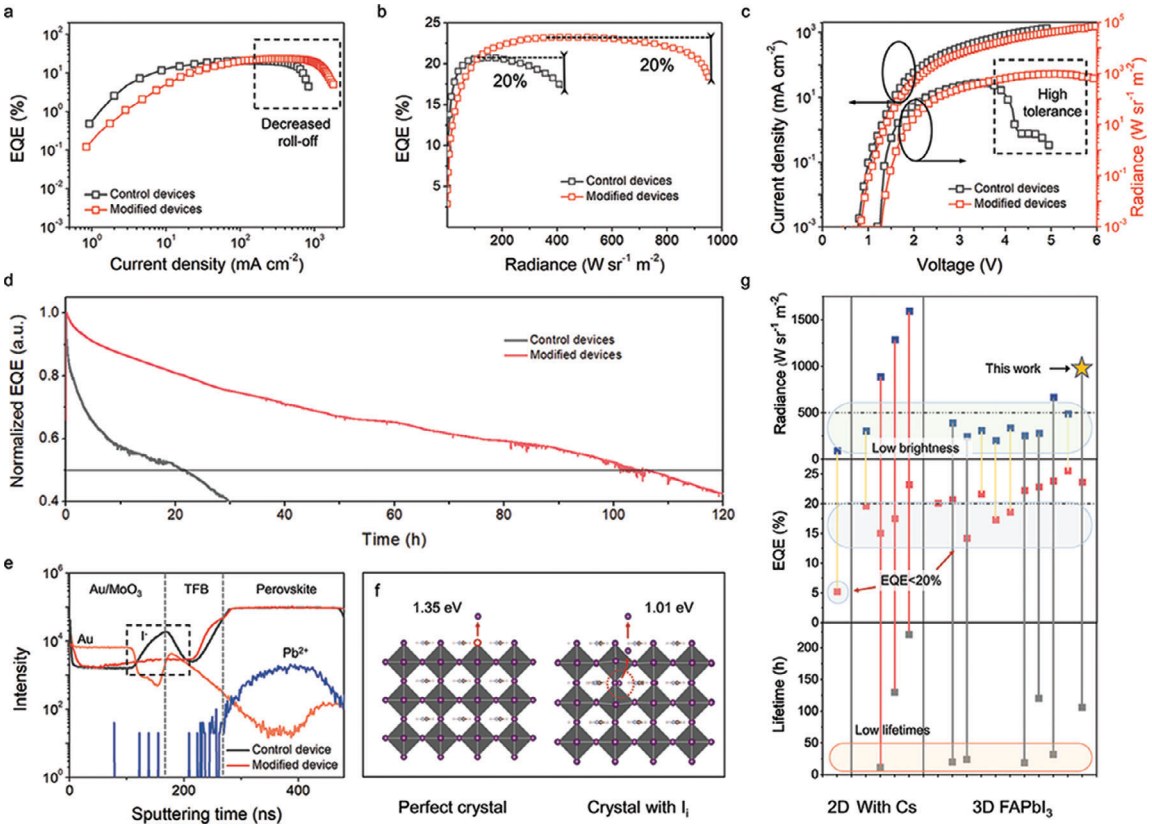

Figure 5. Performance of PeLEDs. a) EQE-current density plots of optimized devices. b) EQE-radiance plots of optimized devices. c) Current density/radiance-voltage plots of optimized devices. d) T_{50} measurement under a constant current density of 100 mA cm^{-2}. e) ToF-SIMS depth profiling of PeLEDs. f) DFT analyses of I^- migration from the perfect perovskite and I_i-existed perovskite. g) Reported peak radiance, peak EQE, and lifetimes under high excitation of PeLEDs in Table S1 (Supporting Information).

3. Conclusion

In this work, we explored the underlying mechanism on the role of excess organic halides in delivering a high efficiency while aggravating the instability of PeLEDs. Experimental and computational results revealed the impact of excess organic halides on the film's physical properties and the resultant device instability. We highlight the significance of the organic halide management and propose a surface clean-assisted cross-linking post-treatment strategy to simultaneously boost the PeLEDs electroluminescence efficiency, brightness, and stability. Systematic experimental and theoretical studies deepen the understanding of the intrinsic instability of perovskite emitters and provide new insights into the rational design of stable and high-efficiency PeLEDs.

Supporting Information

Supporting Information is available from the Wiley Online Library or from the author.

Acknowledgements

G. L. acknowledges the financial support from the Research Grants Council of Hong Kong (GRF Grant Nos. 15221320, 15307922, CRF C7018-20G, C4005-22Y), the Shenzhen Science and Technology Innovation Commission (Project No. JCYJ 20200109105003940), the Hong Kong Innovation and Technology Commission (MHP/020/23), the Hong Kong Polytechnic University (the Sir Sze-yuen Chung Endowed Professorship Fund (8-8480), PRI strategic Grant (1-CD7X), RISE strategic Grant (Q-CDBK)). Dr. Z. R. acknowledges the Hong Kong Polytechnic University Start-up Fund for RAPs under the Strategic Hiring Scheme (BD1H) and the RI-iWEAR Strategic Supporting Scheme (1-CD94). J. T. and G. L. acknowledges the National Key Research and Development Program of China (2023YFE0210600).

Conflict of Interest

The authors declare no conflict of interest.

Data Availability Statement

The data that support the findings of this study are available from the corresponding author upon reasonable request.

Keywords

excess organic ammoniums, ion migration, perovskite light-emitting diodes, post-treatment, stability

Received: December 21, 2023
Revised: April 5, 2024
Published online: April 29, 2024

[1] S. Hou, M. K. Gangishetty, Q. Quan, D. N. Congreve, *Joule* **2018**, *2*, 2421.
[2] Y. Liu, J. Cui, K. Du, H. Tian, Z. He, Q. Zhou, Z. Yang, Y. Deng, D. Chen, X. Zuo, Y. Ren, L. Wang, H. Zhu, B. Zhao, D. Di, J. Wang, R. H. Friend, Y. Jin, *Nat. Photon.* **2019**, *13*, 760.
[3] J. Chen, J. Wang, X. Xu, J. Li, J. Song, S. Lan, S. Liu, B. Cai, B. Han, J. T. Precht, D. Ginger, H. Zeng, *Nat. Photon.* **2021**, *15*, 238.
[4] L. Xu, J. Li, B. Cai, J. Song, F. Zhang, T. Fang, H. Zeng, *Nat. Commun.* **2020**, *11*, 3902.
[5] B. Zhao, Y. Lian, L. Cui, G. Divitini, G. Kusch, E. Ruggeri, F. Auras, W. Li, D. Yang, B. Zhu, R. A. Oliver, J. L. MacManus-Driscoll, S. D. Stranks, D. Di, R. H. Friend, *Nat. Electron.* **2020**, *3*, 704.
[6] Y. Hassan, J. H. Park, M. L. Crawford, A. Sadhanala, J. Lee, J. C. Sadighian, E. Mosconi, R. Shivanna, E. Radicchi, M. Jeong, C. Yang, H. Choi, S. H. Park, M. H. Song, F. De Angelis, C. Y. Wong, R. H. Friend, B. R. Lee, H. J. Snaith, *Nature* **2021**, *591*, 72.
[7] B. Guo, R. Lai, S. Jiang, L. Zhou, Z. Ren, Y. Lian, P. Li, X. Cao, S. Xing, Y. Wang, W. Li, C. Zou, M. Chen, Z. Hong, C. Li, B. Zhao, D. Di, *Nat. Photon.* **2022**, *16*, 637.
[8] Y. Sun, L. Ge, L. Dai, C. Cho, J. Ferrer Orri, K. Ji, S. J. Zelewski, Y. Liu, A. J. Mirabelli, Y. Zhang, J. Y. Huang, Y. Wang, K. Gong, M. C. Lai, L. Zhang, D. Yang, J. Lin, E. M. Tennyson, C. Ducati, S. D. Stranks, L. S. Cui, N. C. Greenham, *Nature* **2023**, *615*, 830.
[9] Z. Li, Z. Ren, Q. Liang, P. Fong, H. Liu, X. Lu, I. Kymissis, G. Li, *Joule* **2024**, *8*, 1176.
[10] Y. Yang, S. Xu, Z. Ni, C. H. Van Brackle, L. Zhao, X. Xiao, X. Dai, J. Huang, *Adv. Mater.* **2021**, *33*, 2100783.
[11] C. Kuang, Z. Hu, Z. Yuan, K. Wen, J. Qing, L. Kobera, S. Abbrent, J. Brus, C. Yin, H. Wang, W. Xu, J. Wang, S. Bai, F. Gao, *Joule* **2021**, *5*, 618.
[12] L. Zhu, H. Cao, C. Xue, H. Zhang, M. Qin, J. Wang, K. Wen, Z. Fu, T. Jiang, L. Xu, Y. Zhang, Y. Cao, C. Tu, J. Zhang, D. Liu, G. Zhang, D. Kong, N. Fan, G. Li, C. Yi, Q. Peng, J. Chang, X. Lu, N. Wang, W. Huang, J. Wang, *Nat. Commun.* **2021**, *12*, 5081.
[13] Z. Liu, W. Qiu, X. Peng, G. Sun, X. Liu, D. Liu, Z. Li, F. He, C. Shen, Q. Gu, F. Ma, H. L. Yip, L. Hou, Z. Qi, S. J. Su, *Adv. Mater.* **2021**, *33*, 2103268.
[14] S. A. Veldhuis, P. P. Boix, N. Yantara, M. Li, T. C. Sum, N. Mathews, S. G. Mhaisalkar, *Adv. Mater.* **2016**, *28*, 6804.
[15] T. Jeon, S. J. Kim, J. Yoon, J. Byun, H. R. Hong, T.-W. Lee, J.-S. Kim, B. Shin, S. O. Kim, *Adv. Energy Mater.* **2017**, *7*, 1602596.
[16] Y. H. Jia, S. Neutzner, Y. Zhou, M. Yang, J. M. F. Tapia, N. Li, H. Yu, J. Cao, J. P. Wang, A. Petrozza, C. P. Wong, N. Zhao, *Adv. Funct. Mater.* **2019**, *30*, 1906875.
[17] Z. Xiao, R. A. Kerner, L. Zhao, N. L. Tran, K. M. Lee, T. Koh, G. D. Scholes, B. P. Rand, *Nat. Photon.* **2017**, *11*, 108.
[18] H. Wang, Z. Chen, F. Tian, G. Zheng, H. Wang, T. Zhang, J. Qin, X. Gao, P. A. van Aken, L. Zhang, X. K. Liu, F. Gao, *Adv. Energy Mater.* **2022**, *13*, 2202185.
[19] T. Liu, X. Zhao, J. Li, Z. Liu, F. Liscio, S. Milita, B. C. Schroeder, O. Fenwick, *Nat. Commun.* **2019**, *10*, 5750.
[20] Y. Deng, Z. Ni, A. Palmstrom, J. Zhao, S. Xu, C. Van Brackle, X. Xiao, K. Zhu, J. Huang, *Joule* **2020**, *4*, 1949.
[21] S. H. Cho, J. Byeon, K. Jeong, J. Hwang, H. Lee, J. Jang, J. Lee, T. Kim, K. Kim, M. Choi, Y. S. Lee, *Adv. Energy Mater.* **2021**, *11*, 2100555.
[22] Z. Zhang, Y. Huang, C. Wang, Y. Jiang, J. Jin, J. Xu, Z. Li, Z. Su, Q. Zhou, J. Zhu, R. He, D. Hou, H. Lai, S. Ren, C. Chen, X. Gao, T. Shi, W. Hu, F. Fu, P. Gao, D. Zhao, *Energy Environ. Sci.* **2023**, *16*, 3430.
[23] T. Cheng, C. Qin, S. Watanabe, T. Matsushima, C. Adachi, *Adv. Funct. Mater.* **2020**, *30*, 2001816.
[24] W. Ding, H. Liu, S. Zhang, D. Qiu, X. Li, S. Wang, *Adv. Funct. Mater.* **2021**, *32*, 2105164.
[25] J. S. Kim, J. M. Heo, G. S. Park, S. J. Woo, C. Cho, H. J. Yun, D. H. Kim, J. Park, S. C. Lee, S. H. Park, E. Yoon, N. C. Greenham, T.-W. Lee, *Nature* **2022**, *611*, 688.
[26] Z. Yuan, Y. Miao, Z. Hu, W. Xu, C. Kuang, K. Pan, P. Liu, J. Lai, B. Sun, J. Wang, S. Bai, F. Gao, *Nat. Commun.* **2019**, *10*, 2818.
[27] G. Zou, Z. Li, Z. Chen, L. Chu, H. L. Yip, Y. Cao, *Adv. Funct. Mater.* **2021**, *31*, 2103219.
[28] Y. Shen, H. Y. Wu, Y. Q. Li, K. C. Shen, X. Gao, F. Song, J. X. Tang, *Adv. Funct. Mater.* **2021**, *31*, 2103870.
[29] Y. Kim, H. Choi, J. Lee, Y. K. Jung, J. Jung, J. Cho, T. Lee, K. Kang, *EcoMat* **2023**, *5*, e12406.
[30] S. H. Cho, J. Byeon, K. Jeong, J. Hwang, H. Lee, J. Jang, J. Lee, T. Kim, K. Kim, M. Choi, Y. S. Lee, *Adv. Energy Mater.* **2021**, *11*, 2100555.
[31] Q.i Wang, Y. Shao, H. Xie, L. u. Lyu, X. Liu, Y. Gao, J. Huang, *Appl. Phys. Lett.* **2014**, *105*, 163508.
[32] Y. Deng, Z. Ni, A. F. Palmstrom, J. Zhao, S. Xu, C. H. V. Brackle, X. Xiao, K. Zhu, J. Huang, *Joule* **2020**, *4*, 1949.
[33] T. Shi, W. Yin, F. Hong, K. Zhu, Y. Yan, *Appl. Phys. Lett.* **2015**, *106*, 103902.
[34] H. Zhang, Z. Ren, K. Liu, M. Qin, Z. Wu, D. Shen, Y. Zhang, H. T. Chandran, J. Hao, C. Lee, X. Lu, Z. Zheng, J. Huang, G. Li, *Adv. Mater.* **2022**, *34*, 2204366.
[35] S. Tan, T. Huang, I. Yavuz, R. Wang, T. W. Yoon, M. Xu, Q. Xing, K. Park, D. K. Lee, C. H. Chen, R. Zheng, T. Yoon, Y. Zhao, H. C. Wang, D. Meng, J. Xue, Y. J. Song, X. Pan, N. G. Park, J. W. Lee, Y. Yang, *Nature* **2022**, *605*, 268.
[36] D. Lin, X. Xu, T. Zhang, N. Pang, J. Wang, H. Li, T. Shi, K. Chen, Y. Zhou, X. Wang, J. Xu, P. Liu, W. Xie, *Nano Energy* **2021**, *84*, 105893.
[37] N. Keller, T. Bein, *Chem. Soc. Rev.* **2021**, *50*, 1813.
[38] M. Smith, John Wiley & Sons, **2020**.
[39] X. Zhao, Z. K. Tan, *Nat. Photon.* **2020**, *14*, 215.
[40] Y. Jia, H. Yu, Y. Zhou, N. Li, Y. Guo, F. Xie, Z. Qin, X. Lu, N. Zhao, *ACS Appl. Mater. Interfaces* **2021**, *13*, 28546.
[41] H. Wang, X. Zhang, Q. Wu, F. Cao, D. Yang, Y. Shang, Z. Ning, W. Zhang, W. Zheng, Y. Yan, S. V. Kershaw, L. Zhang, A. L. Rogach, X. Yang, *Nat. Commun.* **2019**, *10*, 665.
[42] H. Wang, Z. Chen, J. Hu, H. Yu, C. Kuang, J. Qin, X. Liu, Y. Lu, M. Fahlman, L. Hou, X. Liu, F. Gao, *Adv. Funct. Mater.* **2020**, *31*, 2007596.
[43] N. Liu, C. Yam, *Phys. Chem. Chem. Phys.* **2018**, *20*, 6800.
[44] S. Tan, I. Yavuz, M. H. Weber, T. Huang, C. H. Chen, R. Wang, H. C. Wang, J. H. Ko, S. Nuryyeva, J. Xue, Y. Zhao, K.-H. Wei, J. W. Lee, Y. Yang, *Joule* **2020**, *4*, 2426.
[45] S. Wang, Y. Jiang, E. J. Juarez-Perez, L. K. Ono, Y. Qi, *Nat. Energy* **2017**, *2*, 16195.
[46] L. A. Frolova, N. N. Dremova, P. A. Troshin, *Chem. Commun.* **2015**, *51*, 14917.
[47] F. Fu, S. Pisoni, Q. Jeangros, J. Sastre-Pellicer, M. Kawecki, A. Paracchino, T. Moser, J. Werner, C. Andres, L. Duchêne, P. Fiala, M. Rawlence, S. Nicolay, C. Ballif, A. N. Tiwari, S. Buecheler, *Energy Environ. Sci.* **2019**, *12*, 3074.
[48] H. Cho, Y. H. Kim, C. Wolf, H. D. Lee, T. W. Lee, *Adv. Mater.* **2018**, *30*, 1704587.
[49] D. G. Zheng, D. H. Kim, *Nanophotonics* **2023**, *12*, 451.
[50] H. Zhang, Z. Chen, M. Qin, Z. Ren, K. Liu, J. Huang, D. Shen, Z. Wu, Y. Zhang, J. Hao, C. S. Lee, X. Lu, Z. Zheng, W. Yu, G. Li, *Adv. Mater.* **2021**, *33*, 2008487.
[51] X. Li, W. Zhang, Y. Wang, W. Zhang, H. Wang, J. Fang, *Nat. Commun.* **2018**, *9*, 3806.